



OPEN ACCESS

High-yield atmospheric water capture via bioinspired material segregation

Yiwei Gao^{a,b,1} 🗓, Areianna Eason^a, Santiago Ricoy^a, Addison Cobb^a, Ryan Phung^a, Amir Kashani^a 📵, Mario R. Mata^a 📵, Aaron Sahm^a 📵, Nathan Ortiz^c, Sameer Rao^c, and H. Jeremy Cho^{a,1}

Affiliations are included on p. 11.

Edited by Anna Balazs, University of Pittsburgh, Pittsburgh, PA; received December 13, 2023; accepted September 12, 2024

Transforming atmospheric water vapor into liquid form can be a way to supply water to arid regions for uses such as drinking water, thermal management, and hydrogen generation. Many current methods rely on solid sorbents that cycle between capture and release at slow rates. We envision a radically different approach where water is transformed and directly captured into a liquid salt solution that is suitable for subsequent distillation or other processing using existing methods. In contrast to other methods utilizing hydrogels as sorbents, we do not store water within hydrogels—we use them as a transport medium. Inspired by nature, we capture atmospheric water through a hydrogel membrane "skin" at an extraordinarily high rate of 5.50 kg m⁻² d⁻¹ at a low humidity of 35%. and up to 16.9 kg m⁻² d⁻¹ at higher humidities. For a drinking-water application, calculated performance of a hypothetical one-square-meter device shows that water could be supplied to two to three people in arid environments. This work is a significant step toward providing new resources and possibilities to water-scarce regions.

hydrogel | atmospheric water harvesting | convection-limited | water | membrane

With progressive growth of arid areas due to global climate change (1), there is an increasingly dire need for liquid water in water-scarce regions. Water scarcity is a serious global problem that is projected to worsen significantly in the coming decades (2). From a 2016 article (3), around two-thirds of the global population were living under conditions of severe water scarcity for at least one month of the year. In particular, in the southwestern US, water levels are the lowest in 1,200 y (4). Furthermore, inadequately sanitized water sources have led to the spread of diseases such as cholera and typhoid fever, among other water-borne illnesses (5). Thus, technologies that can obtain clean water from alternative water resources are urgently needed. While advances in desalination are highly promising, such technologies cannot be applied to arid regions with limited surface water resources (3, 6, 7). Atmospheric water harvesting (AWH) is an emerging set of approaches to source water from the ambient air as the atmosphere contains 12.9 trillion tons of fresh water, approximately equivalent to 10% of the water in all of the lakes on Earth (8). Arid regions, like much of the southwestern US, are characterized by high temperatures, low rainfall, and low relative humidities. However, existing AWH approaches have low yields and diminishing returns at relative humidities (RH) below 30% (9). In fact, in a recent study (9), Lord et al. determined that if a particular humidity-dependent benchmark in drinking-water harvesting performance (green curve in Fig. 1A, Eq. 10) could be achieved, water could be provided to over one billion people in need, relying entirely on solar power. Yet, no existing current AWH device or approach (orange squares and circles in Fig. 1A) comes close to this benchmark. Other uses for atmospherically sourced liquid water include thermal management applications where the high-latent heat of liquid water can be a useful way to dissipate high heat fluxes (10) such as for data centers with high water usage. Clean hydrogen production can also be produced via water electrolysis sourced from the atmosphere (11). Thus, whether for drinking water or other uses, there is a need to capture atmospheric water into liquid form rapidly.

Atmospheric water harvesting approaches can be broadly divided into two categories: fog collection and vapor condensation (12). The former requires humidities around 100% (6, 13, 14) and geometric structures to gather droplets from airflow or gravity (15, 16) whereas the latter involves condensing ambient water vapor physically using a sorbent material or thermally by cooling below the dew point (17-19). Since the dew point could be below the freezing point at very low humidities, thermal techniques would be challenging to implement in arid regions. Thermal techniques also require

Significance

A layered, convection-limited atmospheric water capture approach is demonstrated, providing water in liquid form at extremely high rates even in low humidities. Inspired by tree frog skins and air plant cuticles, a thin, strong hydrogel acting as a membrane facilitates the transport of water from ambient air into a liquid desiccant for storage. Water in this liquid form is an important precursor for further distillation into drinking water or electrolytic processing for green hydrogen production—enabling new capabilities in arid regions. In addition, pure water can be released from the liquid desiccant using solar energy. Both water capture and release can occur simultaneously, maximizing the potential to harvest water.

Competing interest statement: Y.G., R.P., and H.J.C. are cofounders of a startup company, WAVR Technologies, that has licensed IP from the University of Nevada, Las Vegas relevant to this work. Y.G., R.P., and H.J.C. each own approximately 15% of the startup company, WAVR Technologies. Y.G., R.P., and H.J.C. are inventors on a US patent application filed by the University of Nevada, Las Vegas, on October 28, 2022, that covers the concept of the capture/storage device in this manuscript. The patent is currently pending with application number 63420288. All other authors declare no competing interest.

This article is a PNAS Direct Submission

Copyright © 2024 the Author(s). Published by PNAS. This open access article is distributed under Creative Commons Attribution-NonCommercial-NoDerivatives License 4.0 (CC BY-NC-ND).

Although PNAS asks authors to adhere to United Nations naming conventions for maps (https://www.un. org/geospatial/mapsgeo), our policy is to publish maps as provided by the authors.

¹To whom correspondence may be addressed. Email: yiweig@umich.edu or jeremy.cho@unlv.edu.

This article contains supporting information online at https://www.pnas.org/lookup/suppl/doi:10.1073/pnas.2321429121/-/DCSupplemental.

Published October 22, 2024.

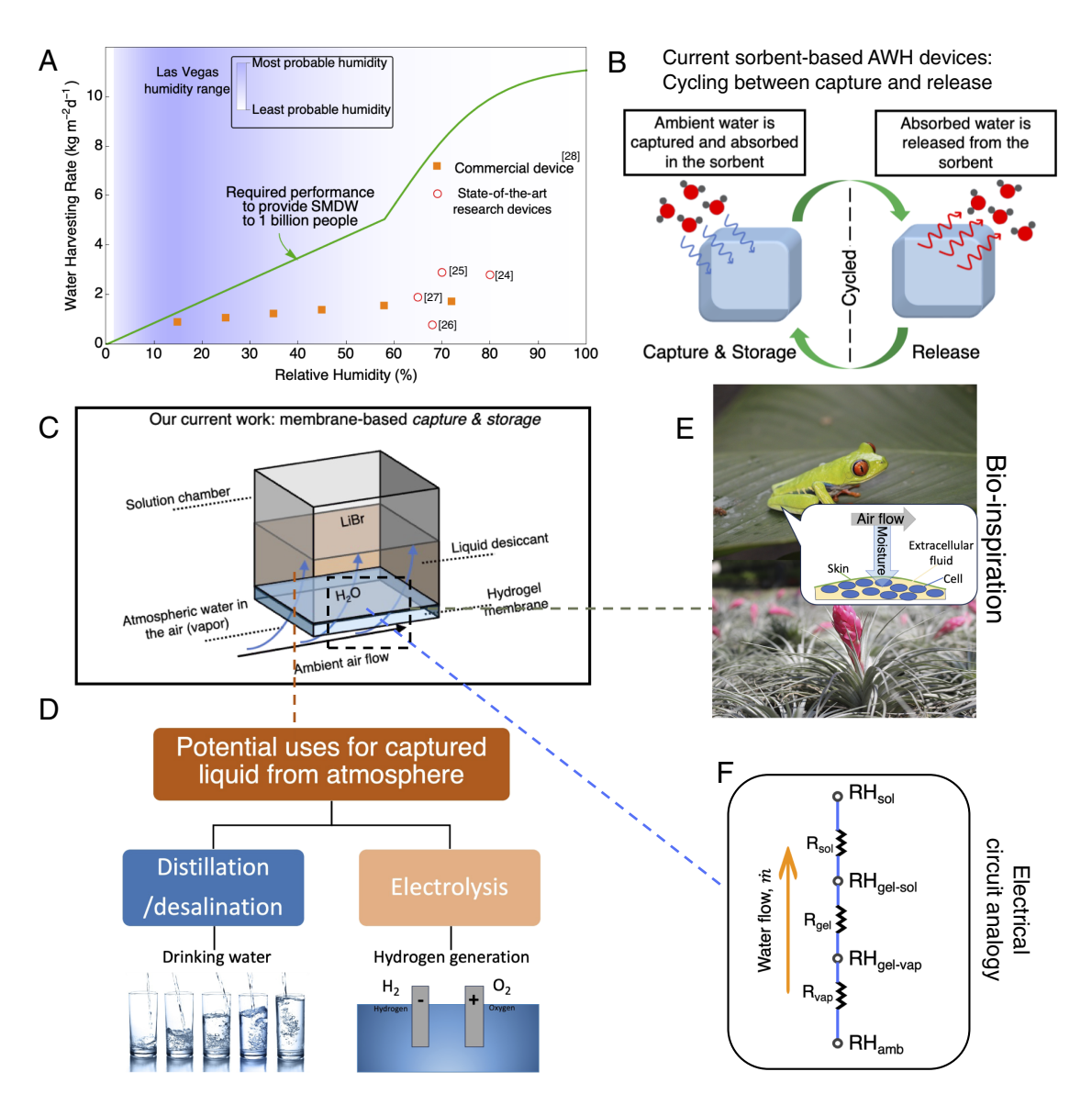


Fig. 1. Our bioinspired water capture and storage concept. (A) Lord et al. modeled the required performance of hypothetical AWH devices that would satisfy the demand of safely managed drinking water (SMDW) for 1 billion people (green line; Eq. 10) (9); however, none of the existing solar-based AWH state-ofthe-art research (24–27) or commercial devices (28) provide this level of performance, especially if operating in an arid area, such as Las Vegas. (B) Current sorbent-based AWH devices use a single monolithic material that can either capture/store or release water at a given time. (C) Here, we develop and present a fast, hydrogel membrane-based capture and storage approach that can be combined with previously demonstrated water release technologies (31-38). (D) The potential uses for captured include distillation for drinking water and electrolysis to generate hydrogen. We envision AWH devices with segregated, multimaterial architectures that can capture, store, and release separately and at the same time. These segregated architectures are bioinspired by (E) tree frogs and Tillandsia "airplants" (29, 30). The rate of water capture is controlled by a mass-transfer process we model using a (F) circuit analogy with a convective resistance in the ambient air (R_{Vap}), a permeation resistance (R_{gel}), and a convective resistance in the liquid solution (R_{Sol}).

significant electrical energy input; however, recent radiative cooling techniques have been demonstrated (20-23) that could enable passive, thermal water harvesting. We focus on passive, athermal vapor condensation that does not require electrical energy input, relying solely on a chemical potential difference to attract water.

Passive vapor-condensation of atmospherically sourced drinking water broadly involves three processes: capture, storage, and release. Water vapor is first captured from the ambient environment is *stored* within a sorbent material. In solid sorbents, the water is inaccessible until it is *released*. This release requires substantial thermal energy (20). As such, current devices utilize solar energy for the release stage, tapping into a free, abundant, and sustainable energy resource for passive operation. Since it is often desirable to utilize solar power for release, the relevant

figure of merit is a water mass flux, j, representing the rate of water moving per unit solar collection footprint. We can describe a flux for capture/storage as well as for release—the harvesting flux would be the minimum of these two. The capture/storage flux, $j_{capture}(RH)$, is dependent on ambient temperature and relative humidity as this sets the chemicalpotential driving force into a sorbent/desiccant whereas the release flux, $j_{\text{release}}(q_{\text{solar}}^{\prime\prime})$, should be dependent on temperature and solar irradiation, q''_{solar} . For non-drinking-water applications, such as electrolysis for hydrogen generation (Fig. 1D), release may or may not be necessary (subsequent processing could occur directly from salt solution). In any case, capture and transformation of atmospheric water vapor at low humidities into liquid form is the primary challenge and the focus of this

Benchmarks and Theoretical Limits. There are useful benchmarks and theoretical limits to understand how effective a given AWH approach is. For drinking water, Lord et al. (9) (shown as the green curve in Fig. 1*A* and plotted globally in *SI Appendix*, Fig. S28) modeled the required performance of a solar-powered, passive AWH approach to provide safely managed drinking water to 1 billion people in varied environmental conditions (RH). However, among the studies we could obtain fluxes for at known humidities, current devices produce only 0.77 kg m⁻² d⁻¹ to 2.89 kg m⁻² d⁻¹ (Fig. 1*A*) (24–27), which are far below the benchmarked requirements, in relatively high RH conditions of 65% to 80% that are hardly representative of the arid climates that urgently require AWH. A commercial device, with performance figures at a wider range of RH conditions, produces similar fluxes at comparable conditions and lower fluxes in arid conditions (28).

We can also understand the low yield of existing AWH devices based on the mismatch in solar-powered AWH fluxes and solar-powered distillation fluxes. Solar-powered distillation techniques (31–38), which have had a surge of interest in the past decade, are a passive means to desalinate water from a salty liquid source (e.g., oceans). These techniques are not as applicable in arid regions since a body of water is required to distill from. However, both solar-powered distillation and existing solar-powered AWH rely on the principle of utilizing solar thermal energy to evaporate and release water with subsequent condensation. Thus, solar distillation provides a useful benchmark to understand the limits of current AWH devices. Solar-powered distillation techniques that utilize localized heating have demonstrated fluxes more than 3.64 kg m⁻² h⁻¹ when fully irradiated by the sun (36–38).

Due to the large differences in flux between current AWH devices and the benchmarked/theoretical limits (Figs. 1 and 5), we believe that current devices are limited by their operational principles and device architectures that do not facilitate high throughput. Current devices utilize a single monolithic, multifunctional sorbent material needing to be cycled between capture and release stages. This single sorbent—whether it be carbonbased sorbents (39-41), deliquescent salts (42-44), a metal organic framework (45-49), zeolite (13, 26), hydrogel (50-54), or liquid desiccant (24, 25)—has to capture, store, and release water all within itself. A common benchmark of sorbents is their water uptake, which quantifies their storage potential a thermodynamic (equilibrium) property. Less discussed in the literature is the absorption/desorption speed of sorbents (transport/kinetics), which quantify the rates of capture and release. Some work by Legrand et al. have revealed, through an experimentally validated mass and energy transfer model, that certain key parameters such as sorbent thickness and porosity can affect adsorption speed significantly (55, 56). In any case, optimizing a single sorbent material to capture and release rapidly, as well as store a large amount, presents substantial material design and synthesis challenges. Furthermore, as this single material can only either perform capture/storage or release at any given time, it must be cycled, limiting the time window to capture and store as much water from the air per day (Fig. 1B). Additionally, water that is stored within solid sorbents is inaccessible and unusable until it is released, precluding the incorporation of highly effective solar distillation techniques that can only be used in the presence of salty liquid solutions. Thus, rather than improving upon existing single-sorbent approaches, we sought a complete redesign of the operation of AWH devices that uses multiple materials. In particular, we looked for ways to decouple the transport/kinetics from equilibrium storage behaviors using nonmonolithic, segregated

materials that can be separately optimized to achieve higher capture fluxes.

Bioinspired Architecture. As opposed to the monolithic, singlematerial sorbent-based approaches, we consider a multimaterial approach where the capture and storage are segregated into separately optimized materials: a hydrogel as a transport medium, and a liquid desiccant as a storage medium. Our approach is inspired by nature where soft membranes [e.g., a tree frog's skin (29) or a cuticle of a *Tillandsia* airplant (30); Fig. 1E] can continuously capture water from the air for hydration (57). These membranes that surround the extracellular fluid act as a protective barrier to the organism, are permeable to water, and facilitate transport of water (58). Meanwhile, the extracellular fluid that the membrane encases stores the water necessary for proper hydration and survival (59). It also serves as a chemical potential sink creating the driving force to draw water from the air through the skin/cuticle into the fluid (capture). As long as the chemical potential of the extracellular fluid is lower than that of the ambient water vapor, the organism will hydrate from the air. In our approach, we mimic this natural design of transport-storage segregation by having a separate transportoptimized capture membrane and a liquid desiccant to provide the chemical potential driving force and liquid storage (Fig. 1*C*).

Using the bioinspired material segregation principle, we envision a vertically integrated, stacked design where a release mechanism on the Top and a capture membrane on the Bottom surround an interstitial storage basin of liquid desiccant (Figs. 1C and 4 A and B). By segregating the location of capture/ storage from release/processing, we can incorporate completely different, separately optimized, and independent processes for capture/storage versus release. For instance, for drinking-water applications, having the liquid desiccant (ionic solution) above the membrane can allow the incorporation of proven, highyield solar distillation/desalination techniques that would otherwise not be compatible with AWH. These solar desalination techniques (31-38) were not originally designed for inland arid regions given the lack of bodies of water. However, with an atmospheric water capture approach that provides a salty liquid solution, a "hidden ocean" can now be provided for these desalination techniques for use inland. Since the highestperforming distillation techniques report water fluxes as high as 3.64 kg m⁻² h⁻¹ under full irradiation (36–38), our goal was to capture water at rates that match or exceed these solar distillation rates; thus, device operation would be limited by available solar power and not capture rate.

Recognizing this need, we focus on attaining the highest capture/storage water fluxes through our material-segregated architecture. In our capture/storage approach, water vapor condenses and permeates through a transport-optimized hydrogel membrane into a liquid desiccant. This desiccant is a saturated lithium bromide (LiBr) salt solution, as its equilibrium relative humidity is around 6% to 8% for typical ambient temperatures (60) (SI Appendix, section 1A). Thus, a saturated LiBr solution will be able to capture water vapor from the ambient down to this low humidity range of <10%, which is lower than other strong desiccant salts such as lithium chloride and sodium hydroxide. LiBr solution also has extremely high uptake that is comparable to the leading hydrogel-based sorbents (52, 61) as we have calculated (SI Appendix, section 9 and Fig. S10). Biofouling is often a concern with membranes; however, the extreme salinity of saturated LiBr solution would most certainly prevent microbial growth (62). Also, lithium is a known microbe inhibitor (63);

thus, it is reasonable to assume that biofouling is not an issue as we apply the highest possible concentration of lithium in the liquid desiccant.

Beneath this solution, we use a hydrogel membrane "skin" to condense and permeate water to the solution from the ambient. We emphasize that this hydrogel membrane, in vast contrast to other hydrogel-based AWH techniques (54, 61, 64-66), does not store water—it simply acts as a transport medium. Thus, water uptake characterizations of our gel membrane are somewhat irrelevant to the water capture performance since the liquid desiccant is providing all of the storage. In any case, we provide water absorption/uptake characterizations of our gel and liquid desiccant (SI Appendix, Figs. S10 and S18) and water uptakes (kg/kg) are comparable to the leading solid sorbents in the literature (52, 61, 67). We use a polyacrylamide hydrogel membrane as we are able to tune its properties to provide several benefits. The hydrogel, being permeable to the solution through its nanoporous polymer network (68), serves as an extension of the liquid desiccant by bringing it in contact to the ambient air. A thorough material characterization of hydrogel properties is included in SI Appendix, section 1B. The hydrogel is also a solid material providing protection from particulate matter with mechanical properties that we tuned to provide flexibility and strength. The high strength of the membrane allows for a large quantity of liquid desiccant to be stored above it with an extremely thin membrane (0.03 mm to 0.7 mm) to optimize transport. Additionally, another motivating factor for using a membrane is that it acts as a physical barrier to the liquid desiccant. The membrane is porous at the polymer mesh scale of around 2.8 nm (detailed calculation is shown in SI Appendix, section 1C), which can block any dust or physical contaminants and enhance the lifetime of the liquid desiccant. As shown in Fig. 1C, water vapor flows from the ambient to the gel-air interface in the direction of lower vapor pressure, then through the hydrogel membrane into the solution chamber. For a drinking water application, we envision that water would be subsequently released from this solution through localized heating, followed by condensation into fresh liquid water. Distiller design would need to incorporate thermal separation between evaporator and condenser sections as we have demonstrated that distillation of saturated LiBr solution is possible in a compact device (SI Appendix, Fig. S30). For a hydrogen generation application, we envision that electrodes placed directly in the solution would allow for electrolytic water splitting for hydrogen generation. In any case, we focus on the capture and storage since subsequent distillation/processing are highly application-specific. Device operation would not be cycled in the typical fashion with monolithic sorbents as capture/storage and release/processing can be occurring independently and simultaneously. We note that the material selection of polyacrylamide hydrogels with lithium salts is not novel to this work as others have employed these materials as sorbents (storage) (54). However, we are innovating from an operational design and device architecture standpoint in that polyacrylamide hydrogels are used as transport media while lithium bromide is used separately as storage—we do not use hydrogels for storage.

Reducing Mass Transfer Resistances. To analyze and develop a fast capture and storage technique, we use an electrical circuit analogy to understand water transport. As shown in Fig. 1F, the mass flow of water, \dot{m} (kg d⁻¹), is analogous to the electrical current. The driving force "voltage" can be represented by the difference in relative humidities between the ambient and the liquid desiccant solution, RH_{amb}-RH_{sol}. Finally, the overall flow

"resistance" is composed of three resistors in series: a convection resistance in the vapor phase, R_{vap} , a liquid diffusion resistance within the gel membrane, $R_{\rm gel}$, and a convection resistance in the liquid solution phase $R_{\rm sol}$. Thus, to maximize the rate of water capture and storage, the "voltage" difference of $RH_{\rm amb}-RH_{\rm sol}$ should be maximized by ensuring the solution is as saturated with LiBr as possible to lower RH_{sol}, and the "resistance" of $R_{\rm vap}+R_{\rm gel}+R_{\rm sol}$ should be as small as possible. To do so, we focused our efforts to model these resistances and determine ways to minimize them.

We can directly calculate the convection resistance in the vapor resistance using the Blasius solution for flow over a flat plate (69) (SI Appendix, section 2). The result is that the water flux is proportional to the square root of the velocity of crossflowing air, *U*, and the difference in relative humidity between the ambient and the gel-air interfacial surface, RH_{amb} - RH_{surf}, as described by the following circuit equation:

$$j = \frac{\dot{m}}{A} = \underbrace{\frac{0.664 D_{\text{w,a}}^{2/3} M_{\text{H}_2\text{O}} P_{\text{sat}} \rho_{\text{air}}^{1/6}}{\mu_{\text{air}}^{1/6} RT} \sqrt{\frac{U}{W}}}_{1/(R_{\text{vap}}A)} \underbrace{\frac{(\text{RH}_{\text{amb}} - \text{RH}_{\text{surf}})}{\text{"voltage" difference}}}_{\text{between ambient and surface.}}$$

Here, A is the surface area of the gel membrane, $D_{w,a}$ is the binary molecular diffusion coefficient of water vapor in air, $M_{\rm H,O}$ is the molar mass of water, P_{sat} is the saturation pressure of water, $\mu_{\rm air}$ is the dynamic viscosity of air, $\rho_{\rm air}$ is the density of air, W is the width of the membrane along the direction of air flow (38 mm for our prototype), R is the molar gas constant, and T is the absolute temperature. The convection resistance is

$$R_{\text{vap}} = \underbrace{\frac{\mu_{\text{air}}^{1/6} RT}{0.664 D_{\text{w,a}}^{2/3} M_{\text{H}_2\text{O}} P_{\text{sat}} \rho_{\text{air}}^{1/6}} \sqrt{\frac{W}{U}} \frac{1}{A}.$$
 [2]

To minimize R_{vap} and maximize mass transfer, the air in the immediate vicinity of the membrane should be as close to ambient humidity as possible. Since, from boundary layer theory, the boundary layer thickness is proportional to $\sqrt{W/U}$, the result indicates that the convection resistance is proportional to the boundary layer thickness. Therefore, placing a membrane in a windy location or using forced convection to minimize boundary layer thickness should increase water capture rate. For scaledup designs, we envision that membrane length, W, be as short as possible to maintain thin boundary layers, which could be achieved by creating wide, linear devices or staggered devices that refresh the boundary layers (SI Appendix, Fig. S2). For this analysis, we assume laminar flow and apply laminar flow in indoor lab experiments (*SI Appendix*, section 1D) for stronger validation. However, the same principles of thin boundary layers enhancing water capture also hold for turbulent flow, which could apply in real, outdoor systems.

We note that this convection resistance would be present in any atmospheric water harvesting device that uses vapor condensation. This is because water vapor, ultimately, is sourced from the air and would need to convect to some surface of an AWH device to be captured. Thus, the fastest possible AWH device is one where all subsequent resistances after R_{vap} are negligible. As a goal of our study, we seek to develop a capture membrane with a resistance, Rgel, that is at least an order of magnitude smaller than R_{vap} so as to be negligible.

To develop a membrane of negligible resistance, we can first derive an expression for $R_{\rm gel}$ to understand how material design parameters affect the transport behavior. Here, we build upon our previous work on the mechanical stiffness, hydraulic permeability, and relative-humidity dependencies of crosslinked hydrogels (68, 70) that is based on semidilute polymer theory (71). Hydrogels are a nanoporous mesh composed of crosslinked polymer strands where the "pores" are the spacing between the strands, which can be described as the mesh size, ξ . Through any porous medium, the mass flow of water is dictated by Darcy's law:

$$j = -\rho_{l} \frac{\kappa}{\mu_{l}} \nabla P, \qquad [3]$$

where ρ_l is the density of liquid water, κ is the hydraulic permeability, μ_l is the dynamic viscosity of liquid water, and ∇P is pressure gradient ($\approx -\Delta P/L$, where L is the thickness of the membrane). As hydrogels are poroelastic materials, the stiffness of a hydrogel (bulk modulus), K, is related to the changes in pressure and volume such that K = VdP/dV (70). Defining a filling fraction, $s \equiv V/V_{\rm wet}$, as the volume of a hydrogel over its wet-state, 100%-RH volume, we can express the change in pressure as

$$dP = \frac{K}{V}dV = \frac{K}{\varsigma}ds.$$
 [4]

Here, s can approach zero for highly deswollen gels and be equal to unity when equilibrated in pure water. In terms of this filling fraction, Darcy's law can be expressed as

$$j = -\rho_{\rm I} \frac{\kappa K}{\mu_{\rm I} s} \nabla s, \qquad [5]$$

where $\nabla s \approx -\Delta s/L$ is the gradient in filling fraction such that water moves from regions of high filling fraction to low filling fraction. We also note that $\kappa K/\mu_l$ is known as the poroelastic diffusion coefficient (72, 73), which describes the diffusion rate of water through poroelastic media. In our previous study (70), we established that the filling fraction is a function of relative humidity, s(RH) (related to the water uptake isotherm), which can be experimentally measured using a vapor sorption analyzer (*SI Appendix*, section 5 and Fig. S18). Expressing the gradient of filling fraction in terms of the dependence on humidity results in the following circuit equation for water flow "current:"

$$j = \frac{\dot{m}}{A} = \underbrace{\rho_{l} \frac{\kappa K}{\mu_{l} s L} \frac{ds}{dRH}}_{1/(R_{gel}A)} \underbrace{\left(RH_{surf} - RH_{sol}\right)}_{\text{"voltage" difference}}.$$
 [6]

Thus, the corresponding resistance within the gel membrane, R_{gel} , is

$$R_{\rm gel} = \frac{\mu_{\rm l} s L}{\rho_{\rm l} \kappa K A} \frac{d \rm RH}{ds}.$$
 [7]

This equation, however, relies on properties that change depending on the humidity. That is, stiffness, K, permeability, κ , and thickness, L, would change with filling fraction, s(RH), which is a function of humidity. As we investigated in detail previously (68), the permeability scales as $\kappa = \kappa_{\text{wet}} s^2$, where κ_{wet} is the experimentally measurable wet-state value. In addition, the stiffness scales as $K = K_{\text{wet}} s^{-9/4}$, where K_{wet} is the experimentally measurable wet-state bulk modulus (70). Finally, it can be shown that for a deswollen hydrogel with a Poisson ratio of 1/3 (74–76), the thickness of the gel membrane when constrained

to constant area, A, is $L = L_{\text{wet}} s^{4/3}$ (SI Appendix, section 3 and Fig. S11). All other parameters do not change with the humidity. Thus, incorporating all of the humidity dependencies into our expression of gel resistance Eq. 7,

$$R_{\text{gel}} = \frac{\mu_{\text{l}}}{\kappa_{\text{wet}} K_{\text{wer}}} \frac{L_{\text{wet}}}{\rho_{\text{l}} A} s^{31/12} \frac{d\text{RH}}{ds}.$$
 [8]

From Eq. 8, we can see that the wet-state permeability and stiffness should be maximized while the thickness should be minimized. Furthermore, highly deswellable gels, such that s is very small at operating conditions, would also minimize R_{gel} due to the $s^{31/12}$ factor. Note that in our expression for R_{gel} , we are assuming uniform properties within the gel membrane. This is valid as long as a poroelastic Peclet number is less than unity, which we justify in *SI Appendix*, section 4. We also reemphasize that the gel membrane does not act as a storage medium; thus, water uptake of the gel itself is not important in determining the storage performance—instead, storage is provided by the desiccant solution, which has similar uptake to the leading hydrogel-based sorbents (52, 61) (SI Appendix, section 9 and Fig. S10). Here, we use the filling fraction s as a convenient gel property to describe its thermodynamic state and not as a water capture performance metric.

Based on our analysis of mass-transfer resistances of the gel, we sought to synthesize hydrogels with minimized filling fraction, s. Compared to a type-I sorbent, type-II and type-III sorbents have much lower filling fraction at typical ambient humidity conditions (SI Appendix, Fig. S19) (77). Thus, we used polyacrylamide hydrogels as they are known to have very strong type-II isotherm behavior (78) with small s at low RH as we experimentally verified previously (70) and for the current work (SI Appendix, Fig. S18). To create thin, 0.03 mm gels, we strengthened the hydrogel using insights gained from a recent study on highly entangled polymer networks with minimal crosslinker (79) (SI Appendix, section 1B). According to their analysis, hydrogels in which entanglement greatly outnumbers crosslinking have significantly higher toughness, strength, and fatigue resistance, compared to traditional crosslinking-dominant hydrogels.

Our gels had a wet-state bulk modulus, $K_{\text{wet}} = 27.6 \pm 0.2 \text{ kPa}$ and a maximum strain of \sim 160% to 200%. The thickness of the gel membranes, when constrained to a fixed area and subjected to the saturated LiBr environment is around L = 0.03 mm. These membranes can withstand the compressive stress associated with \sim 10 cm liquid desiccant above it, equivalent to $\rho gh = 1.4 \,\mathrm{kPa}$, which is much smaller than the compressive strength of the material. Since the membranes are supported by a metal mesh (opening size ~ 0.1 mm), the weight of the liquid can actually cause the gel to deform and bulge out slightly. Using a Young-Laplace stress analysis and applying the tensile strength of 36 kPa, we found that the theoretical maximum height of the liquid before gel failure is around 3 m, corresponding to 1500 kg m⁻² of water storage. The hydraulic permeability of the gels was measured using a custom flow cell (68) to be $\kappa_{\rm wet} = 7.2 \times 10^{-18} \, {\rm m}^2$. With full experimental characterization of our synthesized gels, we were able to directly determine the gel resistance to be $R_{gel} = 0.21 \times 10^6 \, s/kg^{-1}$ using Eq. 8. Compared to the vapor resistance of $R_{\rm vap} = 1.84 \times 10^6 \, {\rm s/kg^{-1}}$, assuming an ambient temperature of $\dot{23}$ °C and cross-flow velocity of $0.3 \mathrm{ms}^{-1}$, R_{gel} was approximately an order of magnitude lower than R_{vapor} . Thus, we hypothesize our gel membranes to have negligible resistance. Furthermore, we calculated the resistance in the solution phase

to be $R_{\rm sol} = 0.093 \times 10^6 \, {\rm s/kg^{-1}}$. This resistance is low due to the Rayleigh-Bénard mixing that occurs from lower-density, lower-salt-concentration liquid at the gel-solution interface (a calculation of R_{sol} is in *SI Appendix*, section 7). Since R_{sol} is lower than R_{vap} by at least one order of magnitude, it is also negligible. From kinetic theory of gases, the resistance due to condensation is also negligible as it is 3 to 4 orders of magnitude smaller than the vapor transfer resistance according to Hertz-Knudsen or Schrage theory. Therefore, the mass transfer in the capture/storage stage should be vapor-convection-limited neither gel-diffusion-limited nor solution-convection-limited where $\dot{m} \approx (RH_{amb} - RH_{sol})/R_{vap}$ since $R_{gel} \ll R_{vap}$. Modeled convection-limited water capture/storage fluxes at ≈ 23 °C (lab conditions) at different air velocities and humidities are shown in SI Appendix, Fig. S12. We also note that the heat generated by the condensation, $jh_{\rm fg}$, is primarily dissipated through the gel and into the solution above it. Applying a Globe and Dropkin natural convection correlation, we calculate that the temperature excursion at the gel-air interface is around 1 degree, which is unlikely to significantly affect chemical driving forces.

Results

To demonstrate our capture and storage approach, we performed a variety of experiments both indoor and outdoor.

Indoor Lab Testing of Convection-Limited Capture/Storage.

To test our expectation of convection-limited behavior, we performed 12 independent indoor capture/storage tests under varied conditions with crossflowing air speeds from 0.3 m s⁻¹ to 0.9 m s⁻¹ and humidities from 10% to 60% (SI Appendix, section 1E; plotted experimental results in Fig. 2C). To facilitate analysis and comparison with established fluid dynamic models, we designed a wind tunnel to provide laminar flow (SI Appendix, section 1D). With negligible gel resistance, the mass flow rate is $\dot{m} \approx (RH_{amb} - RH_{sol})/R_{vap}$, where R_{vap} can be determined

ab initio to predict flow rate (dotted lines in Fig. 2C) according to Eq. 1, where $RH_{surf} = RH_{sol}$. The change of the liquid desiccant volume, ΔV , was determined by photography and image processing. This volume change was converted into captured/stored water mass, m_{capture} (SI Appendix, section 11). Comparing experimental capture/storage rates with predicted rates from Blasius' exact solution for convective flow (SI Appendix, section 2), we found a remarkably close agreement between the results with *no fitting*, confirming convection-limited behavior. As illustrated in the plots, water capture/storage rate increased linearly with ambient relative humidity. Additionally, the rate increased with the square root of wind speed, \sqrt{U} , as expected from Eq. 1. Further enhancement could be provided by turbulent air flow as the boundary layer would become very thin. All tests were performed with 0.1% crosslinking; however, tests with double and half this amount of crosslinking showed no significant change in capture behavior indicating that hydrogel performance is not very sensitive to filling fraction as long as it is low (SI Appendix, section 1F). The close agreement between theoretically predicted flux and experimentally measured flux confirms our hypothesis that the synthesized hydrogels have negligible resistance and that the system is convection-limited.

Outdoor Water Capture/Storage. To demonstrate the potential of our AWH approach in an arid environment, we performed outdoor capture/storage tests locally in Las Vegas (lowest-rainfall metropolitan area in the United States), where the ambient humidity ranges from 20% to 40% in late November. Each outdoor test ran for at least 24 h continuously, and both ambient temperature and humidity changes were recorded as shown in Fig. 3 C and D. We compared our sensor readings of temperature and humidity, which had been calibrated indoors with known salt solutions, with a nearby weather station (KLAS) with publicly available data obtained via Wolfram Mathematica (80) and found good agreement (*SI Appendix*, Fig. S14). Relying only on natural wind to flow across the gel membrane, we measured an average

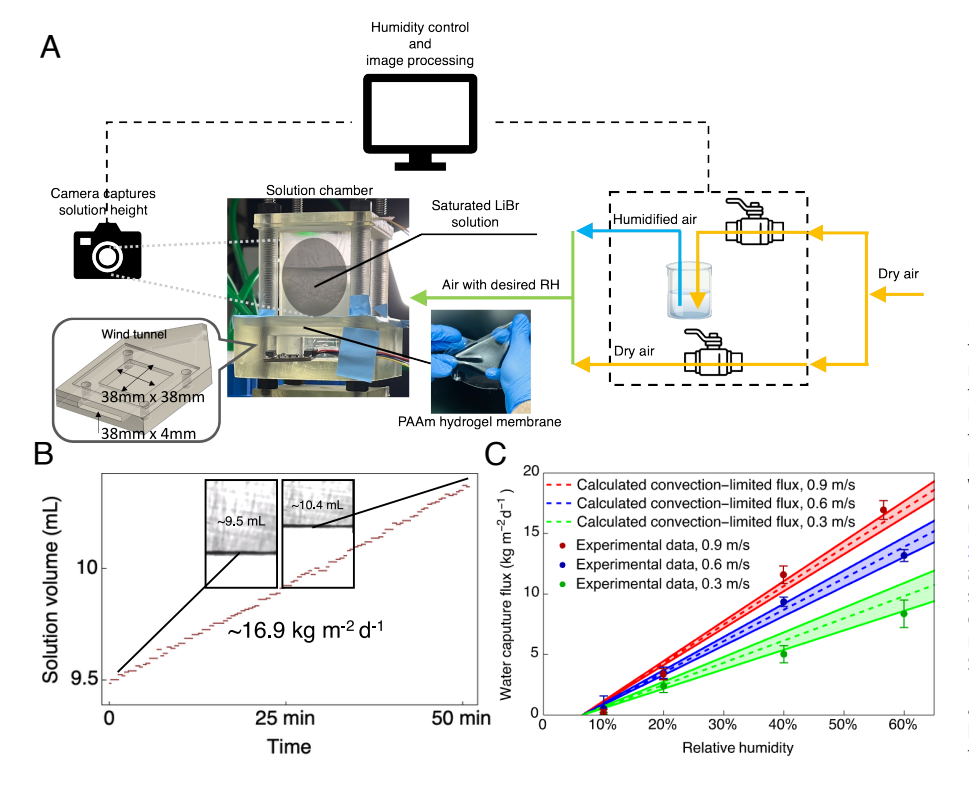


Fig. 2. Lab-controlled water capture/storage tests confirm near-convection-limited performance. (A) A scheme of indoor capture/storage testing. Dry air is first humidified to a desired RH level using PID control. Humidified air with 10% to 60% RH flows into the 3D-printed wind tunnel, located underneath a gel membrane in contact with the liquid desiccant solution above it. (B) A clear volume change of the solution at a steady rate (57%, 0.9 m s⁻¹, 75 min) is shown (Movie S1). (C) Across 12 individual indoor vapor capture/storage tests with varied humidities and wind speeds, all data points collapse along predicted capture/storage rates (dashed lines) within the range of uncertainties in velocity ($\pm 0.07 \,\mathrm{m\,s^{-1}}$ (1 SD); semitransparent areas). Error bars represent 1 SD. The results confirm that the water capture and storage system is operating with convectionlimited behavior and that mass transfer resistance through the gel can be neglected.

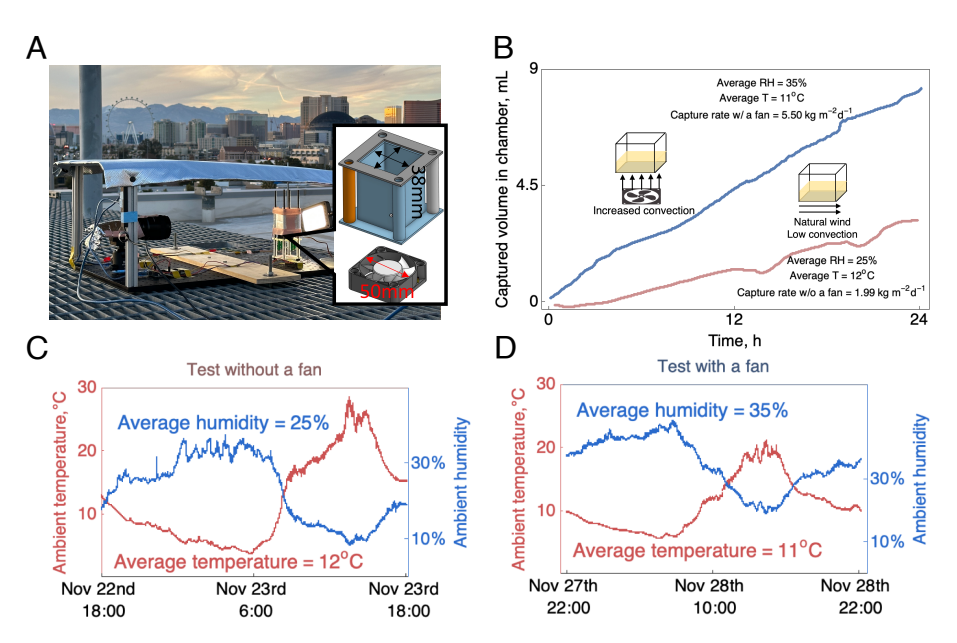


Fig. 3. Outdoor water capture/storage tests demonstrated high water capture and storage in Las Vegas—the driest city in the United States. (A) Outdoor capture/storage testing with a 50 mm diameter fan (generated an effective 0.33 ms⁻¹ wind speed) resulted in (B) 5.50 kg m⁻² d⁻¹ over a 24h period in late November of 2022. Only relying on natural wind without a fan resulted in 1.99 kg m⁻² d⁻¹. Throughout the testing periods, temperature and humidity varied as shown in (C and D)

capture/storage rate of 1.99 kg m⁻²d⁻¹ at an average RH of 25% over a 24-h period (Fig. 3B, red). We note that positive water capture/storage was recorded even as the humidity dipped below 10% (Fig. 3C), demonstrating water capture/storage at the lowest relative humidities compared to other approaches (Fig. 1A). Based on the insight gained from Eq. 2, where mass transfer is inversely proportional to the boundary layer thickness, we incorporated a small 1.4 W fan to apply forced convection over the membrane—combined with the natural wind that day, this effectively provided a wind speed of approximately 0.33 ms⁻¹. (Fig. 3A). The water capture and storage yield increased to 5.50 kg m⁻²d⁻¹ at 35%, representing the highest water yield for any AWH approach at any humidity(24-28). We note that, for the nearby KLAS station weather data, the average wind speed during the 24 h period of both outdoor experiments were 1.24 m/s and 1.47 m/s, respectively, leading to theoretical water capture fluxes as 3.59 kg/m²/d and 6.11 kg/m²/d. It is reasonable that the experimentally measured fluxes are lower than theoretical values since the weather station data were collected at the standard 10 m elevation while the wind to our device was not elevated. We also note that the purpose of adding a fan was simply to demonstrate that water transport is limited by the amount of air convected across the gel.

Releasability Tests. Demonstrating rapid capture/storage rates in our segregated architecture is the main goal of this study as a multitude of release methods could be used [including nonthermal, electrochemical techniques (81)]. Nonetheless, we also sought to demonstrate that the captured/stored water is *releasable* in order to show that our approach is a viable pathway toward atmospheric water harvesting. We performed additional tests to show that the distillation process can occur under the power of sunlight. We also performed limited water quality testing to demonstrate that the captured water can be distilled with trace amounts of lithium and bromide as shown in *SI Appendix*, section 1J. Potable water could be possible with subsequent mineralization.

Solar evaporation with simultaneous capture. To demonstrate that solar evaporation can be incorporated easily into the device architecture, we developed our own release membrane (carbon-

impregnated hydrogel, SI Appendix, section 1B) to absorb and localize solar heat. We placed this membrane on Top of the LiBr solution (Fig. 4C). Using a Class-AAA solar simulator (Ossila) to apply 1 sun of irradiation (1 kW m⁻²) directly over the device provided a mechanism for release while a capture membrane (same as aforementioned capture/storage experiments) and a fan to force ambient air flow was used to capture water from beneath. Further details of the setup are described in *SI Appendix*, section 1H. The fan-powered capture and solar-driven release functions could be independently turned on and off. The first test (Fig. 4 D, Top) individually tested capture and subsequent release. As expected, the liquid level raised during capture (fan on, solar simulator off) and the liquid level decreased during release (fan off, solar simulator on). The capture water flux, j_{capture} , and the release water flux, j_{release} , of the setup were comparable (blue and red regions in Fig. 4 D, Top). As such, when capture and release were operated simultaneously in a subsequent test (fan on, solar simulator on), the volume of the solution in the chamber remained approximately constant (green region in Fig. 4 D, Bottom). Therefore, these results demonstrate that our approach can simultaneously capture and release water as these processes occur independently of one another in a vertically integrated architecture. Additionally, by calculating the actual water capture flux based on reduced chamber dimensions (details in SI Appendix, section 1H), the device successfully captured ambient water at a rate of around 1.42 kg/m²/d at 30% RH, which exceeds the fluxes of state-of-the-art research or commercial devices (24-28).

To further demonstrate that distillation can occur outdoor under the power of sunlight, we utilized a consumer-grade solar water boiler (SolarKettle) mounted on a tracker and set it up on a rooftop (SI Appendix, Fig. S29). We verified that temperatures inside the solar water boiler reached the boiling point of saturated LiBr solution around $\sim 140\,^{\circ}$ C. We also verified that a water mass loss occurs due to evaporation. Using the footprint area of the solar kettle, we determined that 1.9 kg m $^{-2}$ d $^{-1}$ could be released. In a similar outdoor environment, we captured and stored 2.0 kg m $^{-2}$ d $^{-1}$. Thus, our results demonstrate that around 2 kg m $^{-2}$ d $^{-1}$ could be harvested at around 25% humidity on a fall day after the equinox (lower solar potential). However, we

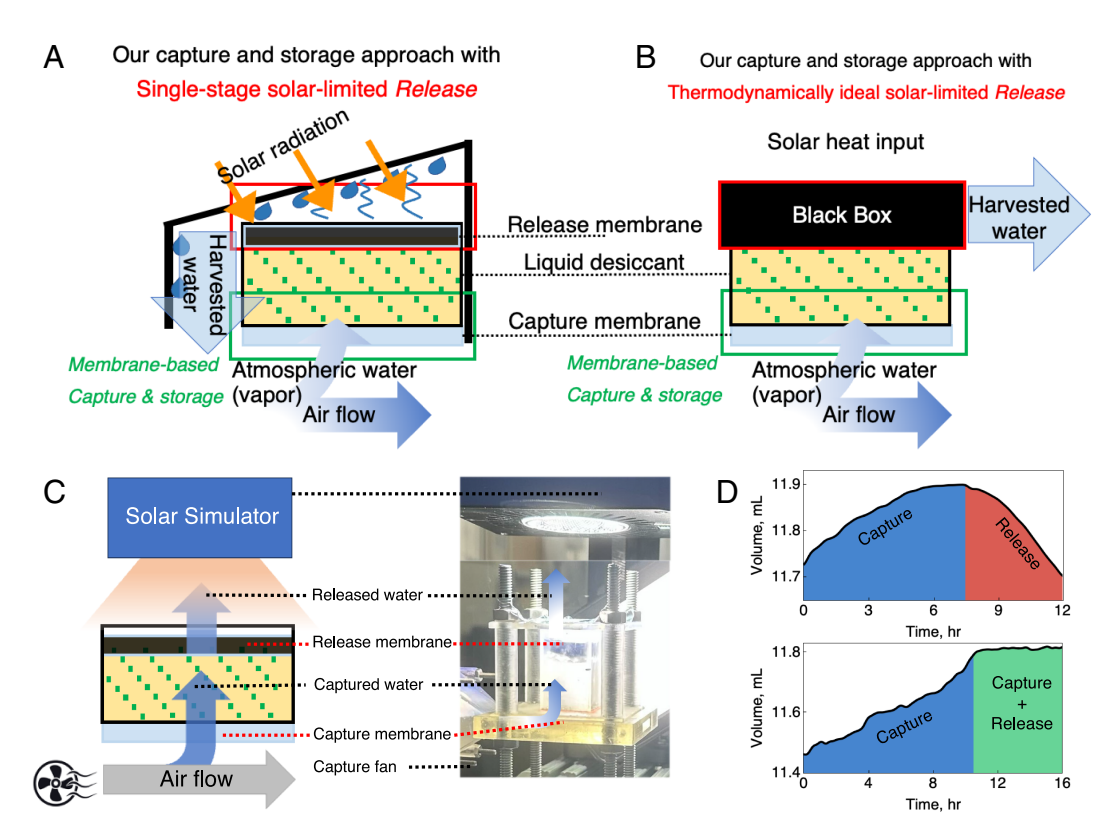


Fig. 4. Envisioned atmospheric water harvesting technology. (*A* and *B*) We envision our capture and storage approach can be coupled with varied release technologies, such as single-stage distillation process (31–38) or a thermodynamically limited distillation device, constitutes a complete AWH system where the harvesting rate is the minimum of capture/storage and release rates. With some verified technologies already approaching the solar limit (36-38), our fast capture/storage approach is an important component that can enable solar-limited AWH. (C) The scheme of the in-lab solar-driven evaporation test on our capture and release setup (Photo of the setup is shown in SI Appendix). (D) Experimental results demonstrated that our refined AWH device was capable of simultaneous water capture and release (Movies S2 and S3).

emphasize that further improvement, to both capture/storage and release, is definitely possible with better solar collection design, and heat and mass transfer optimizations.

Discussion

Both lab and outdoor test results confirm that, through our bioinspired design, water can be captured and stored in liquid salt solution at relative humidities as low as $\sim 10\%$ and at rates that are close to the solar limit of water release at higher humidities. Faster rates can be achieved at higher humidities, and we have recorded as high as 16.9 kg/m²/d at 57% RH, which is a flux that far exceeds the state of the art (24-28) as shown in Fig. 5B, gray points. Faster rates can also be achieved with more convection. Using weather data for 2021 in Las Vegas, we modeled the performance of our AWH capture/storage device using our experimentally verified Eq. 1. Relying only on natural wind (current setup), we modeled a capture/storage rate of 6.6 kg m⁻²d⁻¹ (annual average), which is 88% of the solar limit of $7.5 \text{ kg m}^{-2}\text{d}^{-1}$. Doubling the wind speed either by forced convection or locating the device in a high-wind area (e.g., higher elevations or at constrictions between buildings), we modeled a capture/storage rate of 9.3 kg m⁻²d⁻¹, which is 124% of the solar limit. In any case, coupling our capture/storage approach with a proven release technique would enable a complete AWH package with near-solar-limit performance. A hypothetical onesquare-meter device, with a $W = 38 \,\mathrm{mm}$ width (same as our prototype) could provide individual drinking water [3 kg d⁻¹

(82)] for two to three people in Las Vegas, the driest city in the United States. While the focus of our work is a scientific demonstration of a capture and storage approach, we note that any future scale-up of this device would need to incorporate a release/processing mechanism depending on specific application and consider appropriate mechanical frame design to distribute hydraulic stresses over a large area of gel membrane.

For a drinking-water application, assuming an appropriate release mechanism is incorporated with our capture and storage approach to form a complete AWH device, we calculated the global convection-limited water capture/storage potential of our design based on global weather datasets of temperature, humidity, and wind speed (83, 84) (SI Appendix, Figs. \$23-\$28) as shown in Fig. 5A. In nearly all land regions, the water flux is greater than 10 kg m⁻² d⁻¹. Calculating the performance of our device across the globe (Fig. 5B, blue region) results in the range of water fluxes that generally well exceed Lord's required performance curve to provide safely managed drinking water to 1 billion people (9) (Fig. 5B, green line). In fact, the convection-limited fluxes can exceed the single-stage solar limit (Fig. 5B, red line) and even approach the thermodynamic solar limit for a distillation process (Fig. 5B, black line) (85) (SI Appendix, section 6). Additionally, we calculated the global mapping of water flux needed by an AWH device based on Lord's benchmark (*SI Appendix*, Fig. S28). Apparently, an AWH device that utilizes our capture and storage technology is capable of satisfying the output yield to provide enough safely managed drinking water on a global scale.

Furthermore, our AWH approach has potentially substantial economic advantages—we can estimate a cost of capture and

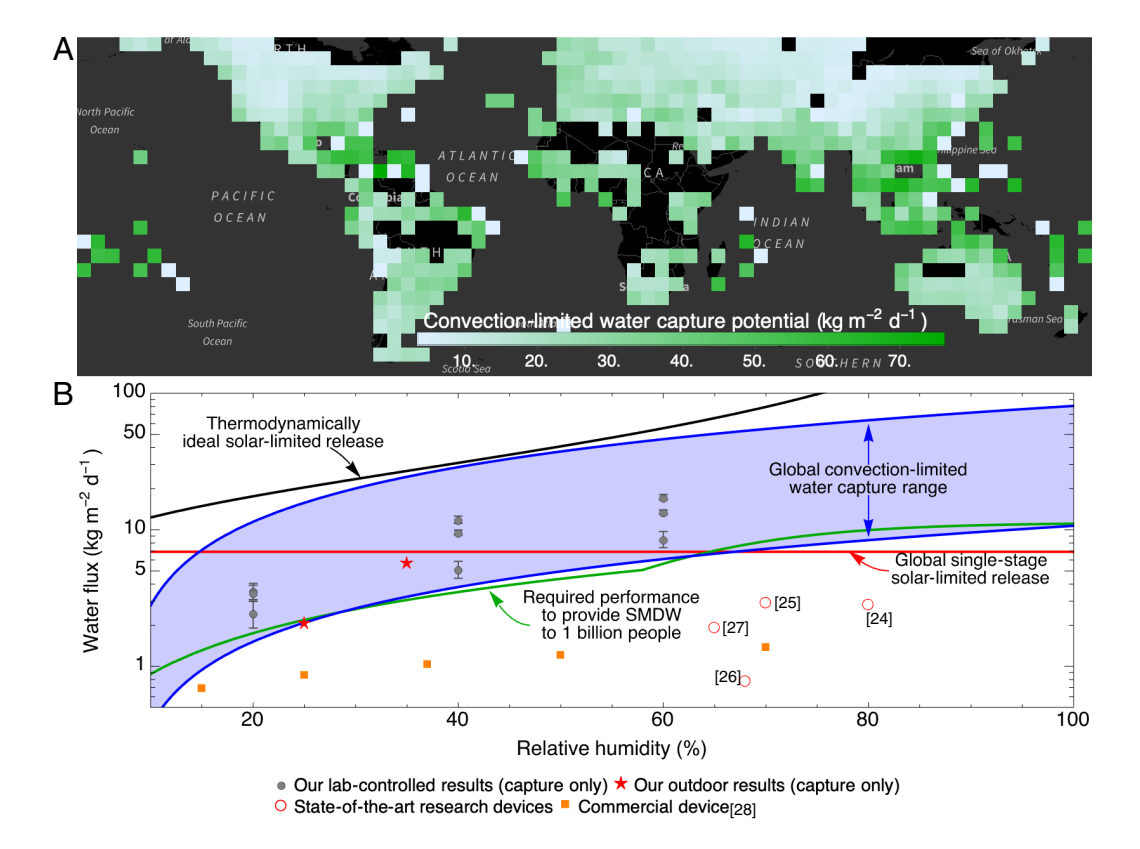


Fig. 5. Global implications of convection-limited water capture and storage. (A) We calculate convection-limited water capture/storage potential globally and find that certain regions can exceed 70 kg m⁻² d⁻¹ (dark green regions). Note that missing pixels are due to incomplete data in the original dataset. (B) Relying on natural wind at 1 m height, convection-limited water capture/storage with our prototype width results in a range of fluxes (blue shaded region representing 95% of the global flux range) that generally exceed the performance required by Lord's benchmark (green curve; Eq. **10**). Error bars represent 1 SD.

storage materials to be approximately \$17 m⁻² or \$1 kg⁻¹ considering only the cost of raw materials purchased at bulk scales, and the combined dry mass of LiBr salt and hydrogel membrane. Thus, high-yield, convection-limited atmospheric water harvesting is highly feasible and could potentially be developed at low cost for wide-scale implementation if the release mechanism could be similarly affordable. In some longer-timescale testing, we have also found that hydrogels are quite robust as we found no observable degradation in capture performance when exposed to LiBr or outdoor environments over the range of a few weeks (SI Appendix, section 1G and Fig. S5). However, further testing on long-term robustness and maintenance is necessary before any technological implementation of this scientific proof of concept. With regard to water production cost, if the device is electrically powered for distillation, we anticipate about 1 kW h L-1 of electricity being required. Applying the average commercial utility rate in the United States, which is approximately 13 cents per kWh, we could expect that every 1 L—this translates to about 13 cents per liter. Alternatively, much or all of this energy could be paid for with solar or waste

Future work will focus on complications that could arise from scaling up (e.g., turbulent wind flows, large membrane fabrication). Future studies will also investigate how additional processes mechanisms could be incorporated to realize a complete AWH or hydrogen generation system. For instance, air filters could be incorporated prior to flowing across gels to prevent any degradation from dust (although no observation degradation was observed in this study). Any solid contaminants that adhere to the gels could be removed through surface cleaning. Reverse osmosis

(RO) could be used to remove any trace contaminants post-distillation. Since this postdistillation water is nearly pure, any RO implementation would be likely straightforward compared to seawater or even tap-water RO. Electrolysis of the solution to generate hydrogen would certainly introduce new challenges to corrosion, necessitating careful electrode material selection [e.g., nickel-based alloys (86)], operational voltages, and electrolytes. While our work, has focused on LiBr, other salts (electrolytes) could be used in principle. For hydrogen generation, NaOH or KOH provides a proven alkaline environment for electrolysis (87) as well as providing low relative humidities (8% to 10%) for water capture.

In summary, we have reimagined the atmospheric water capture process and envisioned a layered architecture resembling the function of skins and cuticles in nature. With this architecture, we are able to segregate the capture, storage, and release of water into separately optimized materials. The architecture also accommodates proven, highly effective water release techniques with near-solar-limit performance for single-stage distillation (36-38). To supply adequate water to the release stage, we have focused on the capture and storage stages and developed a hydrogel membrane "skin" coupled with a liquid desiccant. Using detailed transport and material analysis, we designed the membrane to provide the fastest possible water capture/storage rates as limited by the supply of ambient air flow to the device. This is possible through the use of high entangled polymer networks for high strength, allowing gels to be made extremely thin. Detailed lab and outdoor testing demonstrate that our device has the highest capture/storage fluxes and the largest operational humidities compared to the state of the art. We have modeled the global impact of this convectionlimited performance and have found that, for a drinkingwater application, a hypothetical one-square-meter device could provide daily water needs to several individuals in even the driest environments. Using criteria developed from a previous analysis by Lord et al.(9), implementing a device with convection-limited performance in regions without safely managed drinking water could provide water to over a billion people. Our work could be an important step toward building a scalable and affordable atmospheric water capture device that can provide additional water security to arid communities.

Materials and Methods

Synthesis of Hydrogels. The mixtures of acrylamide monomers, photoinitiator (Irgacure 2959), and crosslinker (N,N'-methylene(bis)acrylamide) were first made as a solution and poured into a mold with 0.5 mm thickness. UV irradiation was applied for 1 h. The crosslinked hydrogel samples were carefully removed from the mold and rinsed to remove unreacted chemicals. All samples were immersed in DI water for 3 d until reaching the equilibrium wet state before use.

Saturated Salt Solution. From Greenspan (60) (SI Appendix, section 1A), the equilibrium relative humidity of saturated LiBr solution is \approx 8% at room temperature. To prepare LiBr saturated solutions, LiBr salt was gradually added into DI water and mixed by a magnetic stirrer, until a solid phase was precipitated. The liquid was allowed to cool after natural exothermic heating from dissolution.

Tensile Testing. We used a custom-built tensile/compression tester used previously (70) to stretch six dog bone-shape hydrogel samples. From stressstrain curves (SI Appendix, Fig. S21), we determined the bulk modulus, Kwet, from the Young's modulus assuming Poisson's ratio is 1/3 (74-76). To ensure the hydrogel samples were tested at their wet state, all tests were finished within 5 min of removal from water.

Permeability Testing. We measured the hydraulic permeability of hydrogel membranes, κ_{wet} , with a custom-built permeability tester used previously (68) (SI Appendix, Fig. S22). In the previous work, we found that the volumetric flow rate, $\it Q$, was linear with $\it \Delta P$ within \pm 2% when $\it \Delta P/K_{
m wet}$ was in the range of 0.5 to 1; thus, we applied a pressure, $\Delta P = 70\%$ $K_{\rm wet}$, by the Elveflow $Microfluidic Flow \, Controller \, and \, recorded \, the \, real-time \, watervolume tric flow \, rate$ for 30 min to calculate the hydraulic permeability of the sample based on Darcy's law. The scheme of the custom-built permeability tester is shown in SI Appendix, Fig. S22.

Indoor Capture and Storage Testing. We used a custom-built wind tunnel with PID control of humidity in the range of 10% to 60% and varied mean velocities from 0.3 m s⁻¹ to 0.9 m s⁻¹. Air flow consideration in the wind tunnel is shown in SI Appendix, section 1D. A camera captured the height of liquid meniscus every 30 s, enabling us to determine the change of saturated solution, V_{change} , in the chamber and calculate the water capture/storage rate over time. The solution humidity was monitored to ensure it remained at \approx 8% during the entirety of the tests. Starting initial volumes were set to be approximately 10 mL. We ensured excess LiBr salt was present to keep the solution saturated at the solubility limit even as additional water was captured and incorporated into the solvent. This also ensured that the chemical-potential driving force remained constant and, thus, capture/storage rates would be approximately constant. Further details of indoor testing procedures are shown in SI Appendix, section 1E and Fig. S13.

Calculation of Captured/Stored Water Mass. As the LiBr solution in the chamber was maintained at saturation, the volume change of the liquid, ΔV , came from both the volume change of saturated solution that consisted of captured water and dissolved salt, and the volume change of undissolved salt.

The mass of captured/stored water, $m_{capture}$, can be calculated as

$$m_{\text{capture}} = \Delta V \frac{(1 - w) \rho_{\text{salt}} \rho_{\text{solution}}}{\rho_{\text{salt}} - w \rho_{\text{solution}}},$$
 [9]

where w is the mass fraction of LiBr in water at the solubility limit, ho_{salt} is the density of LiBr salt, and $\rho_{\rm solution}$ is the density of LiBr saturated solution as a function of temperature. Detailed discussion and derivation are shown in SIAppendix, section 11.

Outdoor Capture and Storage Tests. The outdoor test setup was identical to the indoor setup with the absence of the wind tunnel and humidity control system. We tested with and without a 50 mm computer fan that consumed 1.4 W of electrical power during operation. Each outdoor test was operated on the roof of a laboratory building for at least 24 h continuously. Ambient humidity and temperature were measured and recorded during the entire experiment process for analysis.

Water Sorption Testing. We applied dynamic vapor sorption (DVS) to determine the sorption response of the hydrogel in varied humidities with the DVS Adventure from Surface (SI Appendix, Fig. S15, detailed data are shown in SI Appendix, Figs. S16 and S17). The sample was exposed to progressively lower RH conditions in 10% decrements, with smaller changes when near the saturation point, and allowed to equilibrate at each condition from 98% to 10%. The mass fraction isotherm was fit to a Guggenheim-Anderson-de Boer (GAB) isotherm model (78) (SI Appendix, Fig. S18). Further details of water sorption testing and modeling are shown in *SI Appendix*, section 5 and Figs. S15–S18.

Lord et al.'s Harvesting Performance Benchmark. Lord et al. (9) determined the required specific yield of water to supply one billion people with safely managed drinking water (SMDW) taking into account global data on local population distribution, local solar irradiance, local humidity, and local water need. Humidity-dependent specific yield was expressed in kg of water produced per kWh of solar energy. In our work, we use quantify capture/storage or harvesting performance as a mass flux in kg m⁻² d⁻¹; thus, to convert specific yield to a mass flux, we multiply the specific yield by the global horizontal irradiance (GHI), equivalent to the incoming solar radiation on a flat surface per unit area. In Figs. 1 and 5 (green curve), we take the maximum of the two curves presented by Lord et al., linear and logistic where

$$j_{1\text{billion}} = \max \left(\underbrace{\left(\frac{1.86 \text{ kg kW}^{-1} \text{ h}^{-1}}{\text{Lord's linear curve}} \text{RH}_{\text{amb}'} \right)}_{\text{Lord's linear curve}} \times q_{\text{solar}}'' \right) \times q_{\text{solar}}''$$

$$\underbrace{\frac{2.4 \text{ kg kW}^{-1} \text{ h}^{-1}}{1 + \exp\left(-10.0 \left(\text{RH}_{\text{amb}} - 0.6\right)\right)}}_{\text{Lord's logistic curve}} \right) \times q_{\text{solar}}''}_{\text{I}} \qquad \text{[10]}$$

and $q_{\rm solar}^{\prime\prime}$ is global-average GHI of 4.7 kW h m $^{-2}$ d $^{-1}$. Thus, we are showing a conservative mass flux requirement to supply one billion people with SMDW.

Modeling Location-Specific Water Capture/Storage Potential. Global solar-limited water release was determined using Eq. 11 using global horizontal irradiance data from the Global Solar Atlas 2.0 (88). Convection-limited water capture/storage flux potential was calculated using Eq. 1, where $\mathrm{RH}_{\mathrm{surf}} =$ RH_{amb} , assuming $R_{qel} \ll R_{vap}$. Values for the diffusion coefficient, $D_{w,a}$, were determined using values and an equation from (89). Water and humid air properties were determined using CoolProp (90). Local wind speed data were taken from Wolfram Research (80), while global wind speed data were taken from the Global Wind Atlas (83). 10-m wind speeds were converted to 1-m wind speeds using the power-law wind profile with an exponent of 1/7 (91). Global humidity and temperature data were taken from the HadISDH.blend 1.3.0.2021f version of the Met Office Hadley Centre Integrated Surface Dataset of Humidity (84).

Single-Stage Solar Limit. For a single-stage distillation process (evaporation with subsequent condensation), the solar-limited water release mass flux, $j_{\text{release,single}}$, in kg m⁻² d⁻¹, occurs when irradiation is completely converted into latent heat:

$$j_{\text{release,single}} = \frac{q_{\text{solar}}''}{h_{\text{fg}}}.$$
 [11]

Here, $q_{\rm solar}''$ is the solar irradiation heat flux (W m⁻²), and $h_{\rm fg}$ (J kg⁻¹) is the specific latent heat of vaporization. As noted, the theoretical release flux represented in Eq. 11 can be referenced as a useful benchmark to compare with the capture/storage flux, j_{capture} of a given AWH approach. We also note that purewater h_{fa} is used for reference as this is used to define the standard gained output ratio (GOR) in desalination devices (85)—real devices will have a slightly increased $h_{\rm fq}$ per unit mass of water depending on the sorbent or desiccant used (92) and as we have calculated for lithium bromide (SI Appendix, section 8). In addition, it is noted that Eq. 11 is well below the second-law thermodynamic limits (we calculate the ideal device limit assuming 100% second-law efficiency in Eq. 12 and SI Appendix, section 6). Nonetheless, since actual energy performance will depend on a variety of factors [including "intermediate water" effects (93)], the pure-water h_{fq} represents a convenient reference point that is an approximate estimation of the energy usage for an ideal single-stage distillation process when GOR=1. For instance, using local solar irradiation data in Las Vegas, according to Eq. 11, $j_{\text{release,single}}$ is around 7.5 kg m⁻² d⁻¹ averaged year-round with a maximum of around 12 kg m⁻² d⁻¹ in June, which is more than sufficient to provide one's daily drinking water (2 kg d⁻¹ to 4 kg d⁻¹) (94) for a one-squaremeter device. This single-stage solar limit is a useful target since it would satisfy the benchmark set by Lord et al. (9) to reach one billion people in need for regions with humidities less than 65%.

Solar Limit with Ideal Distillation. For a single-stage distillation system with no heat recovery, the energy required to distill water is the latent heat, as in Eq. **11**. However, in a thermodynamically reversible (100% second-law efficiency; no entropy generation) black box with an inflow of saturated salt solution, the solar heat required, Q_h , to produce a flow of distilled water, \dot{m}_{water} , is

$$\frac{Q_{\rm h}}{\dot{m}_{\rm water}} = \frac{RT_{\rm amb} \ln \left(\frac{1}{\rm RH_{sat}}\right)}{M_{\rm water} \left(1 - \frac{T_{\rm amb}}{T_{\rm h}}\right)},$$
 [12]

where R is the molar gas constant, $T_{\rm amb}$ is the ambient temperature, RH_{sat} is the equilibrium relative humidity of the saturated salt solution, $M_{\rm water}$ is the molar mass of water, and $T_{\rm h}$ is the temperature of the heat source (assumed to be at the boiling point of water at 373 K in Fig. 5B). Note that this result is based on the Gibbs free energy difference from the pure water state and the saturated-salt state, $RT_{\rm amb}$ (1/ $RH_{\rm sat}$), which is in agreement with the recent work by Kocher and Menon (95) where they used thermodynamic activity instead of humidity.

- J. Spinoni et al., How will the progressive global increase of arid areas affect population and land-use in the 21st century? Glob. Planet. Chang. 205, 103597 (2021).
- L. C. Stringer et al., Climate change impacts on water security in global drylands. One Earth 4, 851–864 (2021).
- M. M. Mekonnen, A. Y. Hoekstra, Four billion people facing severe water scarcity. Sci. Adv. 2, e1500323 (2016).
- A. P. Williams, B. I. Cook, J. E. Smerdon, Rapid intensification of the emerging southwestern North American megadrought in 2020-2021. Nat. Clim. Chang. 12, 232-234 (2022).
- H. Jarimi, R. Powell, S. Riffat, Review of sustainable methods for atmospheric water harvesting Int. J. Low Carbon Technol. 15, 253–276 (2020).
- M. J. Kalmutzki, C. S. Diercks, O. M. Yaghi, Metal-organic frameworks for water harvesting from air. Adv. Mater. 30, 1704304 (2018).
- P. Wang, Emerging investigator series: The rise of nano-enabled photothermal materials for water evaporation and clean water production by sunlight. Environ. Sci. Nano. 5, 1078-1089 (2018).
- R. Li et al., Hybrid hydrogel with high water vapor harvesting capacity for deployable solar-driven atmospheric water generator. Environ. Sci. Technol. 52, 11367–11377 (2018).
- J. Lord et al., Global potential for harvesting drinking water from air using solar energy Nature 598, 611–617 (2021).
- J. Zeng et al., Moisture thermal battery with autonomous water harvesting for passive electronics cooling. Cell Rep. Phys. Sci. 4, 101250 (2023).
- 11. J. Guo et al., Hydrogen production from the air. Nat. Commun. 13, 5046 (2022).

Also note that this theoretical device inherently utilizes a Carnot heat engine to produce work: $W=\mathcal{Q}_{\rm h}\,(1-\mathcal{T}_{\rm amb}/\mathcal{T}_{\rm h}).$ For a solar-powered release system, where $\mathcal{Q}_{\rm h}=\mathcal{Q}_{\rm solar}$, the thermodynamically limited mass flux is

$$j_{\text{release,multi}} = \frac{\dot{m}_{\text{water}}}{A} = q_{\text{solar}}'' \left(1 - \frac{T_{\text{amb}}}{T_{\text{h}}}\right) \frac{M_{\text{water}}}{RT_{\text{amb}} \ln\left(\frac{1}{RH_{\text{sat}}}\right)},$$
 [13]

where A is the area of the device, and $q''_{solar} = Q_{solar}/A$. A full derivation is provided in *SI Appendix*, section 6.

Data, Materials, and Software Availability. The data supporting the conclusions of this study are included within the paper text, figures, and *SI Appendix*. Additional data and codes are available at Zenodo (DOI: 10.5281/zenodo.10065172) (96).

ACKNOWLEDGMENTS. We thank Isaac Berk, Jacob Cottino, Angelica Gonzalez-Grado Rooker, Benjamin Sabir, Bianca Navarro, Genaro Marcial-Lorza, and Vesper Evereux for assisting in experiments, designing prototype parts, and providing editing comments to the manuscript. We also acknowledge Haojie Cui for assisting and photographing in the outdoor tests as well as Donghun Pak for early-concept testing. In addition, we appreciate Mark Garner, Joshua Monk, and Douglas Sims for assistance in performing mass spectroscopy and ion chromatography at the College of Southern Nevada. This work was supported by 1) H.J.C. funding from the University of Nevada, Las Vegas through start-up funds, the Faculty Opportunity Award, Technology Commercialization Award, the Top Tier Doctoral Graduate Research Assistantship program, and the Asian American and Native American Pacific Islander-Serving Institution (AANAPISI)the Louis Stokes Alliances for Minority Participation (LSAMP)-McNair Summer Research Institute. 2) H.J.C. the NSF CAREER award under Grant No. 2239416. 3) S. Rao and N.O. the Department of Defense Combat Feeding Research and Engineering Program through the Broad Agency Announcement for Basic and Applied Research at the US Army Combat Capabilities Development Command-Soldier Center through the effort "Metal-Organic Framework based Atmospheric Water Harvesting" (W911QY1910010). This document is approved for public release, Public Affairs Office (PAO) PR2023_81024. 4) N.O. the NSF Graduate Research Fellowship under Grant No. 2139322.

Author affiliations: ^a Department of Mechanical Engineering, University of Nevada-Las Vegas, Las Vegas, NV 89154; ^b Department of Chemical Engineering, University of Michigan, Ann Arbor, MI 48109; and ^cDepartment of Mechanical Engineering, University of Utah, Salt Lake City, UT 84112

Author contributions: Y.G., R.P., and H.J.C. designed research; Y.G., A.E., S. Ricoy, A.C., R.P., A.K., M.R.M., A.S., and N.O. performed research; S. Ricoy contributed new reagents/analytic tools; Y.G. and H.J.C. analyzed data; N.O., S. Rao, and H.J.C. funding; and Y.G. and H.J.C. wrote the paper.

- R. Tu, Y. Hwang, Reviews of atmospheric water harvesting technologies. Energy 201, 117630 (2020).
- A. LaPotin, H. Kim, S. R. Rao, E. N. Wang, Adsorption-based atmospheric water harvesting: Impact of material and component properties on system-level performance. Account. Chem. Res. 52, 1588–1597 (2019).
- X. Zhou, H. Lu, F. Zhao, G. Yu, Atmospheric water harvesting: A review of material and structural designs. ACS Mater. Lett. 2, 671–684 (2020).
- O. Klemm et al., Fog as a fresh-water resource: Overview and perspectives. Ambio 41, 221–234 (2012)
- H. Andrews, E. Eccles, W. Schofield, J. Badyal, Three-dimensional hierarchical structures for fog harvesting. *Langmuir* 27, 3798–3802 (2011).
- M. Eslami, F. Tajeddini, N. Etaati, Thermal analysis and optimization of a system for water harvesting from humid air using thermoelectric coolers. Energy Convers. Manag. 174, 417-429 (2018)
- V. Joshi et al., Experimental investigations on a portable fresh water generator using a thermoelectric cooler. Energy Proced. 109, 161–166 (2017).
- T. Anbarasu, S. Pavithra, "Vapour compression refrigeration system generating fresh water from humidity in the air" in *International Conference on Sustainable Energy and Intelligent Systems* (SEISCON 2011), N. Kumarappan, Albert Singh, M. Srinivasan, Eds. (IET, 2011), pp. 75–79.
- A. K. Rao, A. J. Fix, Y. C. Yang, D. M. Warsinger, Thermodynamic limits of atmospheric water harvesting. *Energy Environ. Sci.* 15, 4025–4037 (2022).

- Z. Huang, X. Ruan, Nanoparticle embedded double-layer coating for daytime radiative cooling. Int. J. Heat Mass Trans. 104, 890-896 (2017).
- X. Xue et al., Creating an eco-friendly building coating with smart subambient radiative cooling. Adv. Mater. 32, 1906751 (2020).
- J. Lee et al., Scalable and efficient radiative cooling coatings using uniform-hollow silica spheres. Appl. Therm. Eng. 254, 123810 (2024).
- H. Qi et al., An interfacial solar-driven atmospheric water generator based on a liquid sorbent with simultaneous adsorption-desorption. Adv. Mater. 31, 1903378 (2019).
- X. Wang et al., An interfacial solar heating assisted liquid sorbent atmospheric water generator. Angew. Chem. 131, 12182–12186 (2019).
- A. LaPotin et al., Dual-stage atmospheric water harvesting device for scalable solar-driven water production. Joule 5, 166–182 (2021).
- V. Ayyagari, Y. Hwang, J. Kim, Design and development of potassium formate based atmospheric water harvester. *Energy* 221, 119726 (2021).
- SOURCE, Technical specification sheet. https://www.scribd.com/document/484400124/SOURCE-Tech-Spec-Sheet. Accessed 24 January 2023.
- C. R. Tracy, N. Laurence, K. A. Christian, Condensation onto the skin as a means for water gain by tree frogs in tropical Australia. Am. Nat. 178, 553-558 (2011).
- P. S. Raux, S. Gravelle, J. Dumais, Design of a unidirectional water valve in Tillandsia. Nat. Commun. 11, 1-7 (2020).
- Commun. 11, 1–7 (2020).
 C. Chen, Y. Kuang, L. Hu, Challenges and opportunities for solar evaporation. *Joule* 3, 683–718 (2019).
- G. Ni et al., Steam generation under one sun enabled by a floating structure with thermal concentration. Nat. Energy 1, 1–7 (2016).
- 33. P. Tao et al., Solar-driven interfacial evaporation. Nat. Energy 3, 1031-1041 (2018).
- M. Gao, L. Zhu, C. K. Peh, G. W. Ho, Solar absorber material and system designs for photothermal water vaporization towards clean water and energy production. *Energy Environ. Sci.* 12, 841–864 (2019).
- Y. Guo et al., Hydrogels and hydrogel-derived materials for energy and water sustainability. Chem. Rev. 120, 7642–7707 (2020).
- Y. Shi, O. Ilic, H. A. Atwater, J. R. Greer, All-day fresh water harvesting by microstructured hydrogel membranes. *Nat. Commun.* 12, 1–10 (2021).
- Y. Guo, F. Zhao, X. Zhou, Z. Chen, G. Yu, Tailoring nanoscale surface topography of hydrogel for afficient solar vapor generation. *Nano Lett.* 19, 2530–2536 (2019)
- efficient solar vapor generation. *Nano Lett.* **19**, 2530-2536 (2019).

 88. F. Zhao et al., Highly efficient solar vapour generation via hierarchically nanostructured gels. *Nat. Nanotechnol.* **13**, 489-495 (2018).
- D. Brassard et al., Improving atmospheric water harvesting in carbon-based sorbents through CO₂ activation. Adv. Sustain. Syst. 8, 2300309 (2024).
- U. Legrand et al., Nanoporous sponges as carbon-based sorbents for atmospheric water generation. Ind. Eng. Chem. Res. 60, 12923–12933 (2021).
- A. S. M. Ali et al., Carbon composites for efficient solar-driven atmospheric water harvesting. J. Environ. Chem. Eng. 12, 113319 (2024).
- M. Ejeian, A. Entezari, R. Wang, Solar powered atmospheric water harvesting with enhanced LiCl /MgSO₄/ACF composite. *Appl. Therm. Eng.* 176, 115396 (2020).
- R. Li, Y. Shi, L. Shi, M. Alsaedi, P. Wang, Harvesting water from air: Using anhydrous salt with sunlight. Environ. Sci. Technol. 52, 5398–5406 (2018).
- Y. Wang et al., Heterogeneous wettability and radiative cooling for efficient deliquescent sorbentsbased atmospheric water harvesting. Cell Rep. Phys. Sci. 3, 100879 (2022).
- N. Hanikel, M. S. Prévot, O. M. Yaghi, MOF water harvesters. Nat. Nanotechnol. 15, 348–355 (2020).
- W. Xu, O. M. Yaghi, Metal-organic frameworks for water harvesting from air, anywhere, anytime. ACS Cent. Sci. 6, 1348–1354 (2020).
- H. Kim et al., Water harvesting from air with metal-organic frameworks powered by natural sunlight. Science 356, 430-434 (2017).
- L. Öhrström, F. M. Amombo Noa, An improved water-harvesting cycle. Science 374, 402–402 (2021).
- Y. Meng, Y. Dang, S. L. Suib, Materials and devices for atmospheric water harvesting. Cell Rep. Phys. Sci. 3, 100976 (2022).
- A. Entezari, M. Ejeian, R. Wang, Super atmospheric water harvesting hydrogel with alginate chains modified with binary salts. ACS Mater. Lett. 2, 471–477 (2020).
- F. Zhao et al., Super moisture-absorbent gels for all-weather atmospheric water harvesting. Adv. Mater. 31, 1806446 (2019).
- Y. Guo et al., Scalable super hygroscopic polymer films for sustainable moisture harvesting in arid environments. Nat. Commun. 13, 1–7 (2022).
- 53. P. A. Kallenberger, M. Fröba, Water harvesting from air with a hygroscopic salt in a hydrogel-derived matrix. *Commun. Chem.* 1, 1–6 (2018).
- H. Lu et al., Tailoring the desorption behavior of hygroscopic gels for atmospheric water harvesting in arid climates. Adv. Mater. 34, 2205344 (2022).
- U. Legrand, P. L. Girard-Lauriault, J. L. Meunier, R. Boudreault, J. R. Tavares, Experimental and theoretical assessment of water sorbent kinetics. *Langmuir* 38, 2651–2659 (2022).
- U. Legrand et al., Fundamental thermodynamic properties of sorbents for atmospheric water capture. Chem. Eng. J. 431, 134058 (2022).
- F. T. Malik, R. M. Clement, D. T. Gethin, W. Krawszik, A. R. Parker, Nature's moisture harvesters: A comparative review. *Bioinspir. Biomim.* 9, 031002 (2014).
- E. Domínguez, J. A. Heredia-Guerrero, A. Heredia, The biophysical design of plant cuticles: An overview. New Phytol. 189, 938–949 (2011).
- Y. Takei, Comparative physiology of body fluid regulation in vertebrates with special reference to thirst regulation. *Jpn. J. Physiol.* 50, 171–186 (2000).
- L. Greenspan, Humidity fixed points of binary saturated aqueous solutions. J. Res. Natl. Bur. Stand. A Phys. Chem. 81, 89 (1977).

- G. Graeber et al., Extreme water uptake of hygroscopic hydrogels through maximized swellinginduced salt loading. Adv. Mater. 36, 2211783 (2023).
- H. Larsen, Halophilic and halotolerant microorganisms-an overview and historical perspective. FEMS Microbiol. Rev. 2, 3–7 (1986).
- L. Cox, D. Dooley, R. Beumer, Effect of lithium chloride and other inhibitors on the growth of Listeria spp. Food Microbiol. 7, 311–325 (1990).
- S. Aleid et al., Salting-in effect of zwitterionic polymer hydrogel facilitates atmospheric water harvesting. ACS Mater. Lett. 4, 511–520 (2022).
- T. Lyu et al., Macroporous hydrogel for high-performance atmospheric water harvesting. ACS Appl. Mater. Interfaces 14, 32433–32443 (2022).
- H. Shan et al., All-day multicyclic atmospheric water harvesting enabled by polyelectrolyte hydrogel with hybrid desorption mode. Adv. Mater. 35, 2302038 (2023).
- T. Li et al., Scalable and efficient solar-driven atmospheric water harvesting enabled by bidirectionally aligned and hierarchically structured nanocomposites. Nat. Water 1, 971–981 (2022)
- Y. Gao, H. J. J. Cho, Quantifying the trade-off between stiffness and permeability in hydrogels. Soft Matter 18, 7735-7740 (2022).
- H. Blasius, Grenzschichten in Flüssigkeiten mit kleiner Reibung (Druck von BG Teubner, Leipzig, 1907).
- Y. Gao, N. K. Chai, N. Garakani, S. S. Datta, H. J. Cho, Scaling laws to predict humidity-induced swelling and stiffness in hydrogels. Soft Matter 17, 9893–9900 (2021).
- P. G. De Gennes, P. G. Gennes, Scaling Concepts in Polymer Physics (Cornell University Press, Ithaca and London, 1979).
- J. F. Louf, N. B. Lu, M. G. O'Connell, H. J. Cho, S. S. Datta, Under pressure: Hydrogel swelling in a granular medium. Sci. Adv. 7, eabd2711 (2021).
- J. F. Louf, S. S. Datta, Poroelastic shape relaxation of hydrogel particles. Soft Matter 17, 3840–3847 (2021).
- H. M. Wyss, T. Franke, E. Mele, D. A. Weitz, Capillary micromechanics: Measuring the elasticity of microscopic soft objects. Soft Matter 6, 4550-4555 (2010).
- E. Geissler, A. M. Hecht, E. Geissler, A. M. Hecht, The poisson ratio in polymer gels. Macromolecules 14, 466-466 (1981).
- D. C. Andrei, B. J. Briscoe, P. F. Luckham, D. R. Williams, Deformation of Gel Particles in Modern Aspects of Colloidal Dispersions (Springer, Netherlands, Dordrecht, 1998), pp. 15–24.
- M. Kajama, N. Nwogu, E. Gobina, Hydrogen permeation using nanostructured silica membranes. Witpress 193, 447–456 (2015).
- H. Mittal, A. Al Alili, S. M. Alhassan, Adsorption isotherm and kinetics of water vapors on novel superporous hydrogel composites. *Microporous Mesoporous Mat.* 299, 110106 (2020).
- J. Kim, G. Zhang, M. Shi, Z. Suo, Fracture, fatigue, and friction of polymers in which entanglements greatly outnumber cross-links. Science 374, 212-216 (2021).
- Wolfram Research, Data from "WeatherData." Wolfram. https://reference.wolfram.com/language/ ref/WeatherData.html. Accessed 27 September 2024.
- Y. Zhang, L. Wang, V. Presser, Electrocatalytic fuel cell desalination for continuous energy and freshwater generation. Cell Rep. Phys. Sci. 2, 100416 (2021).
- SC on the Scientific Evaluation of Dietary Reference Intakes, P on Dietary Reference Intakes for Electrolytes, Water, Dietary reference intakes for water, potassium, sodium, chloride, and sulfate (National Academies Press, 2005).
- N. N. Davis et al., The Global Wind Atlas: A high-resolution dataset of climatologies and associated web-based application. Bull. Am. Meteorol. Soc. 104, E1507–E1525 (2023).
- web-based application. Bull. Am. Meteorol. Soc. 104, E1507–E1525 (2023).
 K. Willett et al., "HadISDH.blend: gridded global monthly land and ocean surface humidity data version 1.3.0.2021f." CEDA Archive. https://doi.org/10.5285/563cb665bc6e43f99b355a9bb8134317. Deposited 26 May 2022.
- JH Lienhard, KH Mistry, MH Sharqawy, GP Thiel, "Chapter 4 thermodynamics, exergy, and energy efficiency in desalination systems" in *Desalination Sustainability*, H. A. Arafat, Ed. (Elsevier, Amsterdam), pp. 127–206 (2017).
- N. M. Kubo, F. Ketter, S. Palkovits, R. Palkovits, Nickel and commercially available nickel-containing alloys as electrodes for the electrochemical oxygen evolution. *ChemElectroChem* 11, e202300460 (2024)
- K. Zeng, D. Zhang, Recent progress in alkaline water electrolysis for hydrogen production and applications. *Prog. Energy Combust. Sci.* 36, 307–326 (2010).
- Solargis, "Global Solar Atlas 2.0." Global Solar Atlas. https://globalsolaratlas.info/. Accessed 24 January 2023.
- T. L. Bergman, A. S. Lavine, F. P. Incropera, D. P. DeWitt, Fundamentals of Heat and Mass Transfer (Wiley Global Education US, Hoboken, 2018), vol. 8.
- I. H. Bell, J. Wronski, S. Quoilin, V. Lemort, Pure and pseudo-pure fluid thermophysical property evaluation and the open-source thermophysical property library coolprop. *Ind Eng. Chem. Res.* 53, 2498–2508 (2014).
- 91. J. S. Touma, Dependence of the wind profile power law on stability for various locations. J. Air Pollut. Control Assoc. 27, 863–866 (1977).
- H. Kim et al., Characterization of adsorption enthalpy of novel water-stable zeolites and metalorganic frameworks. Sci. Rep. 6, 19097 (2016).
- X. Zhou, F. Zhao, Y. Guo, B. Rosenberger, G. Yu, Architecting highly hydratable polymer networks to tune the water state for solar water purification. Sci. Adv. 5, eaaw5484 (2019).
- National Academies of Sciences, Engineering, and Medicine, Dietary Reference Intakes for Water, Potassium, Sodium, Chloride, and Sulfate (The National Academies Press, Washington, DC, 2005).
- J. D. Kocher, A. K. Menon, Addressing global water stress using desalination and atmospheric water harvesting: A thermodynamic and technoeconomic perspective. Energy Environ. Sci. 16, 4983–4993 (2023).
- Y. Gao, H. J. Cho, Data from "Data for high yield atmospheric water capture via bioinspired material segregation." Zenodo. https://doi.org/10.5281/zenodo.10065172. Deposited 2 November 2023.